Rapid Scan EPR Imaging as a Tool for Magnetic Field Mapping

Oxana Tseytlin[1,3] · Andrey A. Bobko[1,3] · Mark Tseytlin[1,2,3]

Abstract

Functional four-dimensional spectral–spatial electron paramagnetic imaging (EPRI) is routinely used in biomedical research. Positions and widths of EPR lines in the spectral dimension report oxygen partial pressure, pH, and other important parameters of the tissue microenvironment. Images are measured in the homogeneous external magnetic field. An application of EPRI is proposed in which the field is perturbed by a magnetized object. A proof-of-concept imaging experiment was conducted, which permitted visualization of the magnetic field created by this object. A single-line lithium octa-n-butoxynaphthalocyanine spin probe was used in the experiment. The spectral position of the EPR line directly measured the strength of the perturbation field with spatial resolution. A three-dimensional magnetic field map was reconstructed as a result. Several applications of this technology can be anticipated. First is EPRI/MPI co-registration, where MPI is an emerging magnetic particle imaging technique. Second, EPRI can be an alternative to magnetic field cameras that are used for the development of high-end permanent magnets and their assemblies, consumer electronics, and industrial sensors. Besides the high resolution of magnetic field readings, EPR probes can be placed in the internal areas of various assemblies that are not accessible by the standard sensors. Third, EPRI can be used to develop systems for magnetic manipulation of cell cultures.

✉ Mark Tseytlin
mark.tseytlin@hsc.wvu.edu

1   Department of Biochemistry, West Virginia University, Morgantown, WV 26506, USA

2   West Virginia University Cancer Institute, Morgantown, WV 26506, USA

3   In Vivo Multifunctional Magnetic Resonance Center at Robert C. Byrd Health Sciences Center, West Virginia University, Morgantown, WV 26506, USA

1 Introduction

Functional electron paramagnetic resonance (EPR) imaging has been successfully used in a wide range of biomedical studies [1–14]. Besides the distribution of spin probes, spatial distributions of several tissue microenvironment markers, such as oxygen partial pressure, pH or redox status have been measured [2, 5, 15–21]. Functional information is encoded into an additional spectral and/or temporal dimension [22, 23]. As a result, the images become four or even five dimensional [24]. Rapid scan (RS) EPR is the method of choice for spectral–spatial imaging, especially when multi-line spin probes are used. This technique demonstrates higher sensitivity in comparison with the conventional first-derivative continuous wave (CW) EPR [1, 2, 9, 24–34]. RS spectra can be captured on a microsecond time scale. Thousands of projections can be measured within a very small-time interval, which is an imprortant factor for 4D imaging. In comparison with pulsed EPR, the RS method is not limited by bandwidth and relaxation times. As a result, multi-functional multi-line spin probes can be used.

Conventional EPR imaging requires that the external magnetic field is homogenous. If this condition does not hold, corrections have to be made during data processing and/or image analysis to avoid erroneous results. This manuscript explores an experimental situation in which the distribution of the static magnetic field across the sample volume is inhomogeneous by design. The field inhomogeneity is not caused by the magnet or imperfect gradient coils. It is generated by the sample itself. A proof-of-concept experiment is described in this manuscript, in which a small magnetic particle was used to perturb field homogeneity. Magnetic field distribution around this particle is imaged using a spin probe with a narrow EPR line. The spectral line position in a given voxel directly reads the value of the local field generated by the particle.

RS EPRI mapping of the magnetic field, both constant (DC) and low-frequency AC, can be used in a wide range of applications, such as in the development of high-end permanent magnets and sensors based on these magnets. In this case, EPR can be used as an alternative to commercial magnetic field scanners. Another potential application is co-registration with magnetic particle imaging (MPI) modality [35]. EPR can provide superior spatial resolution and help independently track the movement of magnetic nanoparticles in vivo. The proposed method of magnetic field mapping may be used as an imaging tool to design and test devices for magnetic cell manipulation [36].

2 Sample Preparation

Iron oxide Fe_3O_4 silicon-coated nanoparticles, 20–30 nm, were purchased from US Research Nanomaterials Inc. Dry nanoparticle powder was placed on a Teflon plate, and ethyl cyanoacrylate liquid glue (Loctite Super Glue, Henkel Corp., Dusseldorf, Germany) was added to the powder to completely soak it in the glue. A second Teflon plate was placed on the top of the sample with a gap of 500 μm

between the plates. As a result, a solid film was formed after the glue dried. A square with the dimensions of 700 µm × 700 µm was cut of the film that was used in the imaging experiments. The final dimensions of the magnetic sample were 700 µm × 700 µm × 500 µm.

Lithium octa-n-butoxynaphthalocyanine (LiNc-BuO) microcrystals were the imaging agents. The conventional use of this probe is for longitudinal oxygen measurements in pre-clinical and clinical EPR applications [37–41]. For magnetic field mapping described in this paper, LiNc-BuO spin probe was homogeneously dispersed in a resin ('Clear' resin, FLGPL CL04, Formlabs, Somerville, MA) at 0.5 mg/mL concentration. This resin, which is used in the commercial Formlabs 3D printers, polymerizes after irradiation of a violet light source (405 nm). The polymerization process depletes oxygen dissolved in the resin so that the formed solid sample becomes completely deoxygenated. Full-width half-magnitude EPR linewidth of the deoxygenated LiNc-BuO was measured to be 0.1 G.

A hole (inner diameter 11 mm) was made in the Teflon plate (8 mm thickness) that was half-filled with the resin-probe mixture. Light exposure caused polymerization of the resin. The magnetic sample was placed on the top of the polymerized substance, and the liquid resin was added to fill the hole. After light exposure, the entire sample was polymerized with the magnetic particle surrounded by LiNc-BuO probes in the solid matrix. The sample was removed from the Teflon plate and imaged.

3 EPR Imaging Results

Locally built modular EPR system operating at 800 MHz was used [1] for 4D spectral–spatial imaging. All measurements were done in the rapid scan mode. A total of 2546 projections were acquired per image, including intermediate 26 zero-gradient spectra. These spectra were used to correct for a slow drift of the external magnetic field caused by a temperature-sensitive permanent magnet. Gradient coils embedded into the magnet cause heating and a slow field drift as a result. RS signals were transformed into absorption EPR spectra using a previously developed algorithm [42]. The scan frequency was 9400 kHz. Scan amplitude was varied depending on the gradient value to maximize signal-to-noise ratios of projections. The maximum gradient value of 3 G/cm was used to measure projections. Images were reconstructed using a previously described algorithm [22] developed by Komarov et. al. [5] The result of reconstruction was a 4D array (three spatial and one spectral coordinate). Each voxel containing a spectrum was line fitted using a standard MATLAB function. The line position parameters were extracted to form 3D images of magnetic field distributions.

The magnetic field map was reconstructed that is shown in Fig. 1. Six cross sections along the z-direction of the external magnetic field are presented. Figure 1 is in a good qualitative agreement with the field distribution around a magnetic dipole (see Fig. 2). Figure 2 schematically places cross sections in Fig. 1 in the corresponding regions of the dipole field. The white area in the cross section (see Fig. 1d)
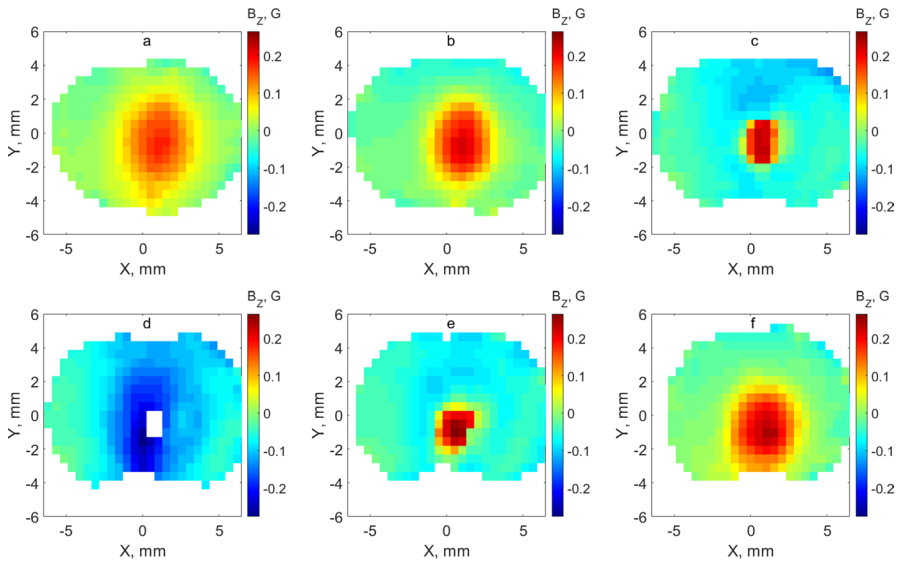
Fig. 1 Cross sections of magnetic field map along the z-axis parallel to the external magnetic field. Z-coordinates of the 2D slices were − 3 mm, − 2 mm, − 1 mm, 0 mm, 1 mm, 2 mm for a, b, c, d, e, and f sections, respectively

Fig. 2 Sketch of magnetic field produced around a magnetized object containing iron nanoparticles. Regions corresponding to cross sections {a, b, c, d, e, f} in Fig. 1 are depicted
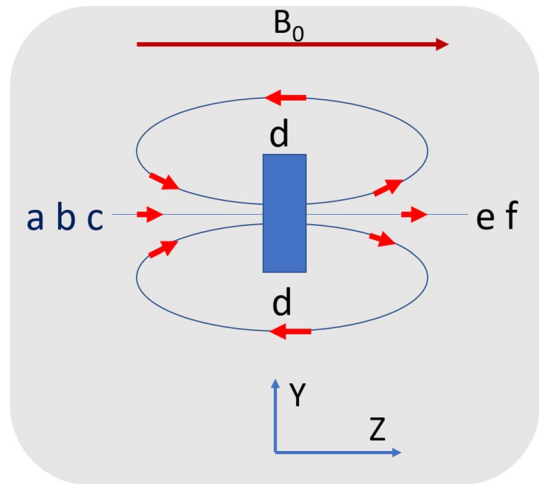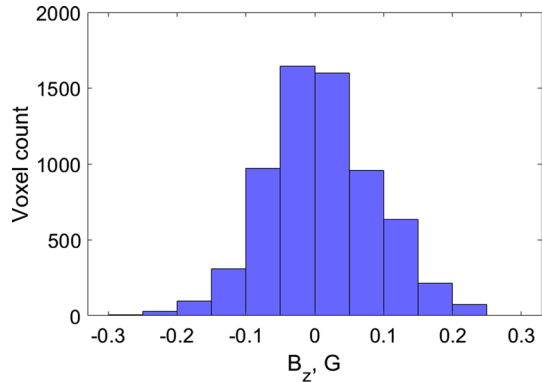
Fig. 3 Histogram of magnetic field values for the entire image. The bin size is 0.05 G

corresponds to the position of the magnetized object. Figure 3 shows the distribution of the magnetic field values within the entire image.

4 Discussion

EPR imaging was demonstrated as a method to map the static magnetic field produced by the magnetized assembly of iron nanoparticles. Measurements were done at 800 MHz, which for LiNc-BuO probe corresponds to the magnetic field strength of approximately 256 G. Alternating field scans did not exceed 6 G in peak-to-peak amplitude, so that the particles were magnetically saturated, and the scans did not significantly affect their magnetization. If an object is magnetized in the strong external magnetic field, as in the described here experiment, only the field component parallel to that field (B_z in Fig. 2) can be imaged. Re-orientation of the object in the magnet will change the direction of the magnetization vector which will remain to be aligned with the external field. If the magnetized sample is not magnetically isotropic, anisotropic properties of this sample can be imaged. It is also possible to image the magnetic field created by a magnetized object that retains its magnetization in the absence of an external force. In this case, components in the plane orthogonal to the excitation alternating field can be measured. Repositioning of a resonator or cavity with respect to the sample can be used to create a complete vector map around the magnetized object.

EPR imaging has the potential to occupy an application niche that cannot be claimed by MRI, superconducting quantum interference devices (SQUID), and similar techniques that can measure very weak fields but may become impractical for the measurements requiring a large dynamic range. In principle, given the current RS state-of-the-art, magnetic field distributions as wide as 150 G can be imaged. This range can be extended by combining slow external field sweep with fast scans [43]. Since MRI operates at much higher compared to EPRI magnetic fields, the placement of a magnetized object that creates such strong fields may not only be impractical but also dangerous. The maximum sample size will depend on the resonator type and radiofrequency, RF. Using relatively low RF, such as 250 MHz, will permit

imaging objects several centimeters in size. However, the use of low frequency will restrict the range of magnetic fields that can be imaged.

Several applications can be anticipated. First is the co-imaging with MPI. EPRI can be used to visualize and track magnetic nanoparticles that are routinely used in pre-clinical studies. Toward this goal, maps similar to one shown in Fig. 1 can be used. By solving an inverse deconvolution problem, the distribution of nanoparticles can be obtained. EPRI may be able to compete and/or be complementary to MPI. For example, particle position and pH mapping can be done simultaneously, as hyperfine splitting will not be affected. The entire EPR spectrum will be offset by induced magnetization so that relative line positions will be preserved. Testing various types of devices and sensors based on small permanent magnets will be a potential industrial application of this technology. In this case, EPRI will become an alternative to the currently used magnetic field cameras. This method has the advantage of imaging the interior of the objects while scanners collect data outside. EPRI field mapping can also be used to design and test devices for magnetic cell manipulation [36].

The described approach to imaging of the magnetic field distribution is not limited to RS EPR. The standard first-derivative CW method can be used as well. However, rapid-scan images can be acquired much faster given the same magnetic field map resolution. RS EPR was demonstrated to provide superior sensitivity when probes with long relaxation times are used [30]. Magnetic field imaging based on pulsed EPR may not be practical if wide magnetic field distributions are measured. In this case, the free induction decay signal may be very short to be adequately captured. Also, RS EPR may be used to image time-dependent periodic AC magnetic fields. RS EPR can capture a single projection within tens of microseconds. Synchronizing imaging acquisition with the scan frequency will permit measurements of AC fields.

Author Contributions Oxana Tseytlin: Instrumentation development; Sample preparation; Imaging data acquisition.
Andrey Bobko: EPR probe synthesis.
Mark Tseytlin: Idea; Image reconstruction and processing.

Data Availability Magnetic field map can be provided as a MATLAB 3D structure.

Code Availability Not applicable.

Compliance with Ethical Standards

Conflict of interest The authors declare that they have no known competing financial interests or personal relationships that could have appeared to influence the work reported in this paper.

References

1. O. Tseytlin, P. Guggilapu, A.A. Bobko, H. AlAhmad, X. Xu, B. Epel, R. O'Connell, E.H. Hoblitzell, T.D. Eubank, V.V. Khramtsov, B. Driesschaert, E. Kazkaz, M. Tseytlin, J. Magn. Reson. **305**, 94 (2019)
2. M. Poncelet, B. Driesschaert, O. Tseytlin, M. Tseytlin, T.D. Eubank, V.V. Khramtsov, Bioorg. Med. Chem. Lett. **29**(14), 1756 (2019)
3. M.C. Emoto, H. Sato-Akaba, Y. Matsuoka, K.I. Yamada, H.G. Fujii, Neurosci. Lett. **690**, 6 (2019)
4. M. Gonet, B. Epel, H.J. Halpern, M. Elas, Cell Biochem. Biophys. **77**(3), 187 (2019)
5. D.A. Komarov, Y. Ichikawa, K. Yamamoto, N. Stewart, S. Matsumoto, H. Yasui, I.A. Kirilyuk, V.V. Khramtsov, O. Inanami, H. Hirata, Anal. Chem. **90**(23), 13938 (2018)
6. H. Yasui, T. Kawai, S. Matsumoto, K. Saito, N. Devasahayam, J.B. Mitchell, K. Camphausen, O. Inanami, M.C. Krishna, Free Radic. Res. **51**(9–10), 861 (2017)
7. B. Epel, M. Krzykawska-Serda, V. Tormyshev, M.C. Maggio, E.D. Barth, C.A. Pelizzari, H.J. Halpern, Cell Biochem. Biophys. **75**(3–4), 295 (2017)
8. H. Kubota, D.A. Komarov, H. Yasui, S. Matsumoto, O. Inanami, I.A. Kirilyuk, V.V. Khramtsov, H. Hirata, MAGMA **30**(3), 291 (2017)
9. B. Epel, S.V. Sundramoorthy, M. Krzykawska-Serda, M.C. Maggio, M. Tseytlin, G.R. Eaton, S.S. Eaton, G.M. Rosen, J.P.Y. Kao, H.J. Halpern, J. Magn. Reson. **276**, 31 (2017)
10. X. Wang, M. Emoto, Y. Miyake, K. Itto, S. Xu, H. Fujii, H. Hirata, H. Arimoto, Bioorg. Med. Chem. Lett. **26**(20), 4947 (2016)
11. M. Hashem, M. Weiler-Sagie, P. Kuppusamy, G. Neufeld, M. Neeman, A. Blank, J. Magn. Reson. **256**, 77 (2015)
12. H.B. Elajaili, J.R. Biller, M. Tseitlin, I. Dhimitruka, V.V. Khramtsov, S.S. Eaton, G.R. Eaton, Magn. Reson. Chem. **53**(4), 280 (2015)
13. M. Elas, J.M. Magwood, B. Butler, C. Li, R. Wardak, R. DeVries, E.D. Barth, B. Epel, S. Rubinstein, C.A. Pelizzari, R.R. Weichselbaum, H.J. Halpern, Cancer Res. **73**(17), 5328 (2013)
14. V.V. Khramtsov, J.L. Zweier, Functional in vivo EPR Spectroscopy and Imaging Using Nitroxide and Trityl Radicals, in *Stable Radicals: Fundamentals and Applied Aspects of Odd-Electron Compounds*, ed. by R. Hicks (John Wiley and Sons Ltd, Chichester, 2010), pp. 537–566
15. S. Kishimoto, K.I. Matsumoto, K. Saito, A. Enomoto, S. Matsumoto, J.B. Mitchell, N. Devasahayam, M.C. Krishna, Antioxid. Redox Signal **28**(15), 1378 (2018)
16. V.V. Khramtsov, A.A. Bobko, M. Tseytlin, B. Driesschaert, Anal. Chem. **89**(9), 4758 (2017)
17. B. Epel, M.K. Bowman, C. Mailer, H.J. Halpern, Magn. Reson. Med. **72**(2), 362 (2014)
18. G. Redler, M. Elas, B. Epel, E.D. Barth, H.J. Halpern, Adv. Exp. Med. Biol. **789**, 399 (2013)
19. T. Yokoyama, A. Taguchi, H. Kubota, N.J. Stewart, S. Matsumoto, I.A. Kirilyuk, H. Hirata, J. Magn. Reson. **305**, 122 (2019)
20. H. Sato-Akaba, M.C. Emoto, H. Hirata, H.G. Fujii, J. Magn. Reson. **284**, 48 (2017)
21. J. Goodwin, K. Yachi, M. Nagane, H. Yasui, Y. Miyake, O. Inanami, A.A. Bobko, V.V. Khramtsov, H. Hirata, NMR Biomed. **27**(4), 453 (2014)
22. D.A. Komarov, H. Hirata, J. Magn. Reson. **281**, 44 (2017)
23. M.M. Maltempo, S.S. Eaton, G.R. Eaton, J. Magn. Reson. **72**(3), 449 (1987)
24. U. Sanzhaeva, X. Xu, P. Guggilapu, M. Tseytlin, V.V. Khramtsov, B. Driesschaert, Angew. Chem. Int. Ed. Engl. **57**(36), 11701 (2018)
25. J. Moser, K. Lips, M. Tseytlin, G.R. Eaton, S.S. Eaton, A. Schnegg, J. Magn. Reson. **281**, 17 (2017)
26. S.S. Eaton, Y. Shi, L. Woodcock, L.A. Buchanan, J. McPeak, R.W. Quine, G.A. Rinard, B. Epel, H.J. Halpern, G.R. Eaton, J. Magn. Reson. **280**, 140 (2017)
27. M. Tseytlin, B. Epel, S. Sundramoorthy, D. Tipikin, H.J. Halpern, J. Magn. Reson. **272**, 91 (2016)
28. J.R. Biller, D.G. Mitchell, M. Tseytlin, H. Elajaili, G.A. Rinard, R.W. Quine, S.S. Eaton, G.R. Eaton, J. Vis. Exp. **115**, 54068 (2016)
29. Z. Yu, R.W. Quine, G.A. Rinard, M. Tseytlin, H. Elajaili, V. Kathirvelu, L.J. Clouston, P.J. Boratynski, A. Rajca, R. Stein, H. McHaourab, S.S. Eaton, G.R. Eaton, J. Magn. Reson. **247**, 67 (2014)
30. D.G. Mitchell, M. Tseitlin, R.W. Quine, V. Meyer, M.E. Newton, A. Schnegg, B. George, S.S. Eaton, G.R. Eaton, Mol. Phys. **111**, 2664 (2013)
31. D.G. Mitchell, G.M. Rosen, M. Tseitlin, B. Symmes, S.S. Eaton, G.R. Eaton, Biophys. J. **105**(2), 338 (2013)
32. H. Sato-Akaba, M. Tseytlin, J. Magn. Reson. **304**, 42 (2019)

33. M. Tseytlin, A.V. Stolin, P. Guggilapu, A.A. Bobko, V.V. Khramtsov, O. Tseytlin, R.R. Raylman, Phys. Med. Biol. **63**(10), 105010 (2018)
34. O. Tseytlin, A. Bobko, M. Tseytlin, in *Proceedings of the 59th Annual Rocky Mountain Conference on Magnetic Resonance*, (Snowbird, Utah, United States, 22-27 July 2018), p. 87
35. J.W.M. Bulte, Adv. Drug Deliv. Rev. **138**, 293 (2019)
36. F. Leonard, B. Godin, Methods Mol. Biol. **1406**, 239 (2016)
37. H. Hou, N. Khan, S. Gohain, M.L. Kuppusamy, P. Kuppusamy, Biomed. Microdevices **20**(2), 29 (2018)
38. J. Frank, D. Gundel, S. Drescher, O. Thews, K. Mader, Free Radic. Biol. Med. **89**, 741 (2015)
39. M.M. Kmiec, D. Tse, J.M. Mast, R. Ahmad, P. Kuppusamy, Biomed. Microdevices **21**(3), 71 (2019)
40. H. Hou, N. Khan, P. Kuppusamy, Adv. Exp. Med. Biol. **977**, 313 (2017)
41. L.A. Jarvis, B.B. Williams, P.E. Schaner, E.Y. Chen, C.V. Angeles, H. Hou, W. Schreiber, V.A. Wood, A.B. Flood, H.M. Swartz, P. Kuppusamy, in *Proceedings of the Xth International Workshop on EPR in Biology and Medicine* (Krakow, Poland, 2-6 October 2016), p.34
42. M. Tseytlin, J. Magn. Reson. **281**, 272 (2017)
43. Z. Yu, T. Liu, H. Elajaili, G.A. Rinard, S.S. Eaton, G.R. Eaton, J. Magn. Reson. **258**, 58 (2015)